



## One-step hydrothermally synthesized ferrite@polymeric nanoparticles for decolorization of crystal violet

Hassan Alijani<sup>a</sup>, Mostafa Hossein Beyki<sup>b</sup>, Reyhaneh Kaveh<sup>c</sup>, Yousef Fazli<sup>d,\*</sup>

<sup>a</sup>Department of Chemistry, Faculty of Science, Shahid Chamran University of Ahvaz, Ahvaz, Iran, email: alijani.hassan89@gmail.com

<sup>b</sup>School of Chemistry, University College of Science, University of Tehran, Tehran, Iran, email: hosseinbakim@gmail.com

<sup>c</sup>Chemistry Department, Sharif University of Technology, Tehran, Iran, email: reyhanehkaveh@yahoo.com

<sup>d</sup>Department of Chemistry, Faculty of Science, Arak Branch, Islamic Azad University, Arak, Iran, Tel./Fax: +98 86 33670017; emails: yousef.fazli@gmail.com, y-fazli@iau-arak.ac.ir

Received 13 May 2017; Accepted 20 January 2018

### ABSTRACT

An efficient dye decolorization platform was developed through one-step hydrothermally route based on magnetic polymeric resin and employed in aqueous crystal violet (CV) adsorption. The polymer nanohybrid composed of ZnFe<sub>2</sub>O<sub>4</sub> and hydroxybenzoic acid–resorcinol resin as metal and organic fragment, respectively. Several techniques such as X-ray diffraction, N<sub>2</sub> – adsorption desorption, vibration sample magnetometer, field emission scanning electron microscopy and Fourier transform infrared spectroscopy were employed for characterization of as-prepared nanohybrid. CV adsorption showed low equilibrium time within 10 min with the adsorption capacity of 83.3 mg g<sup>-1</sup>. Regeneration of the sorbent performed by methanol–HNO<sub>3</sub> solution. The thermodynamic study revealed that adsorption follows the endothermic path as well as it is spontaneous.

*Keywords:* Crystal violet; Decolorization; Polymer; Resin

### 1. Introduction

Synthetic dyes are extensively presented in the effluent water from textile, leather, rubber, plastic and dyestuff industry. Dye attendance in the environment, generate high toxicity and disturbances in the aquatic ecosystem since they prevent penetration of light into the water as well as deplete the dissolved oxygen [1–4]. In addition, the dye decolorization is difficult owing to the presence of conjugated aromatic backbone and various chromophore on their structure. Moreover, some intermediates were produced by hydrolysis and oxidation of dye which makes them mutagenic and carcinogenic [5,6]. Up to now, gentian violet or crystal violet (CV) as a cationic triphenylmethane dye widely employed for temporary hair coloring, dyeing cotton, as well as ink and dermatological agent. Importantly, skin contact and inhalation of CV are harmful moreover, causes cancer to human beings.

Moreover, it persists in various environments since it is non-biodegradable, and poorly metabolized by microbes [7–10].

There are many conventional physicochemical methods for dye removing such as reduction, membrane filtration, ion exchange, chemical precipitation, reverse osmosis and adsorption. Among these methods adsorption process has been recognized as an attractive separation technique since; adsorption is a low cost, efficient and simple design method which does not produce waste by-products [11–13]. In the recent decade, the scientific researchers have focused on searching for more efficient materials in order to manipulate the water pollution. As a result, various types of adsorbents including agricultural waste, rice husk, sawdust, sugarcane bagasse, opal and activated carbon have been successfully employed for dye removing [14–19]. Even though the materials showed advantages, but they suffer the main drawback of difficulty in regeneration. As a result, selection of a proper adsorbent is still very important in the aforementioned method, since it affects the efficiency of the methods.

\* Corresponding author.

Recently, it was found that nanotechnology can obviate many issues about the water quality. In other words, inimitable routes provided by nanomaterials can dispel the problematic topic involved with pollutants in the efficient and cost-effective way [20]. Hence, various nanosorbents such as ZnO, TiO<sub>2</sub>, MCM-41,  $\gamma$ -alumina, nickel nanoparticles, zeolite and zeolite-based composites have been proposed in this outline [21–28].

Recently, smart hydrogels, especially phenolic resins, are largely employed for preparing various nanostructured carbons for adsorption of dyes. Smart hydrogels with three-dimensional cross-linked structure are able to retain water and solute molecules. In fact, the characteristics and adsorption capability of hydrogels depend on the presence of the hydroxyl and carboxyl functional groups [29,30]. However, some of these materials are not proving to be good adsorbents due to lower adsorption rate. This limitation can be eliminated by hybrid nanocomposites with inorganic materials by using cavitation during the synthesis [31]. Among various types of inorganic reinforcing materials, metal oxides especially magnetic ferrite nanoparticles not only allow higher adsorption capacity for cationic dyes, but also facilitate the nanohybrid separation from solution by a simple external magnetic field [32–34].

In this research, a novel magnetic phenol-formaldehyde resin has been synthesized and employed for removing aqueous CV. The nanohybrid was synthesized by one-step hydrothermal process as it consists of ZnFe<sub>2</sub>O<sub>4</sub> nanoparticles and hydroxybenzoic acid-resorcinol fragments. Dye adsorption characteristics such as equilibrium time, adsorption capacity and temperature dependence behavior were investigated and optimized.

## 2. Experimental

### 2.1. Materials and instruments

Resorcinol, 4-hydroxybenzoic acid, paraformaldehyde, NaOH, Zn(NO<sub>3</sub>)<sub>2</sub>·6H<sub>2</sub>O, FeCl<sub>3</sub>·6H<sub>2</sub>O and ammonia (25% w/w) were supplied from Merck (Darmstadt, Germany). Working solutions of CV were obtained by dilution of 1,000 mg L<sup>-1</sup> solution. The crystallinity and surface morphology of prepared magnetic particles were studied by powder X-ray diffraction (XRD) and field emission scanning electron microscope (FE-SEM) using a Phillips powder diffractometer, X'Pert MPD and HITACHI S 4160 instruments. An Equinox 55 Bruker spectrometer was used to measure Fourier transform infrared (FTIR) spectra with attenuated total reflectance (ATR). The N<sub>2</sub> adsorption-desorption isotherms and magnetization measurement were performed on a Nova Station A system, and a vibration sample magnetometer (VSM; Model 7400, Lake Shore Cryotronics, Inc., Westerville, OH). The pH adjustment was performed with a digital pH-meter (model 692, metrohm, Herisau, Switzerland). Dye adsorption properties were recorded with a Lambda-25 UV-Vis spectrophotometer.

### 2.2. Synthesis of magnetic resin

A one-step hydrothermal route has been employed for preparing ZnFe<sub>2</sub>O<sub>4</sub>@polymeric resin. For this purpose, 0.5 g of resorcinol and 0.5 g of hydroxybenzoic acid was dissolved

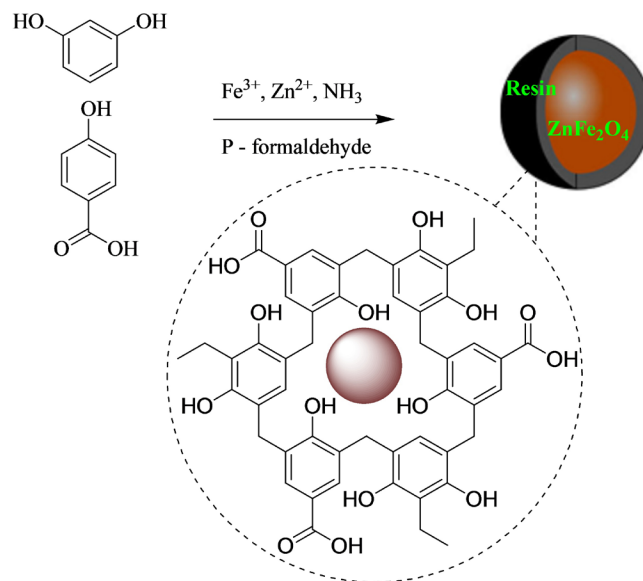


Fig. 1. Synthetic route to prepare magnetic resin.

in 25 mL of distilled water containing 3 mL of concentrated NH<sub>3</sub> (25% w/w). Thereinafter, 1.12 g of FeCl<sub>3</sub>·6H<sub>2</sub>O and 0.6 g of Zn(NO<sub>3</sub>)<sub>2</sub>·6H<sub>2</sub>O in 10 mL of distilled water have been added to the above solution and stirred for 5 min. In a subsequent step, 0.5 g of *p*-formaldehyde has been added to the mixture and the pH of them was adjusted to 12 with NaOH. After stirring for 30 min, the reactants were transferred into a Teflon lined autoclave and heated at 150°C for 24 h. After the reaction, the suspension was filtered and washed with distilled water three-time and with ethanol twice. The resulted gray products were dried at 70°C for 6 h. Synthetic protocol is schematically illustrated in Fig. 1. The same protocol was employed for the synthesis of ferrite nanoparticles and polymer.

### 2.3. Dye adsorption experiment

Dye adsorption experiment has been performed in 50 mL sample solutions (0.1–40 mg L<sup>-1</sup>). The pH of the samples has been adjusted to 8.0 and after adding 30 mg of the nanohybrid, the mixtures have been shaken for 10 min. After the equilibrium, the CV concentration in the supernatants or in the eluted phase has been determined by measuring the peak intensity at  $\lambda = 590$  nm using the UV-Vis spectrophotometer.

## 3. Results and discussion

### 3.1. Characterization of the nanohybrid

The XRD pattern of resin (Fig. 2(a)) shows typical main peaks at  $2\theta = 29.64^\circ, 35.48^\circ, 35.7^\circ, 44.2^\circ, 52.72^\circ, 56.2^\circ, 61.76^\circ$  and  $75.1^\circ$  corresponding to (220), (311), (222), (400), (422), (511), (440) and (535) planes of zinc ferrite structure [35]. As well as the XRD pattern showed a main broad scattering with a maximum height at  $17^\circ$  which confirmed the preparation of magnetic resin. It was obvious that the growth of the resin not changed the crystalline behavior of ZnFe<sub>2</sub>O<sub>4</sub> nanoparticles. Scherrer equation was employed to determine the average crystallite size of polymer nanocomposite.

$$D = (0.9\lambda)/(\beta \cos\theta) \tag{1}$$

In this equation  $D$  is the average crystal size,  $\lambda$  (0.1540589 nm) is the X-ray wavelength used,  $\beta$  (0.00165) is the angular line width of half maximum intensity in radians and  $\theta$  (17.82) is Bragg's angle expressed in degree. According to this equation, the average size of 88.4 nm was obtained for polymer nanocomposite.

In the FTIR spectrum of nanocomposite (Fig. 2(b)), peaks at 3,342 and 2,940  $\text{cm}^{-1}$  are attributed to the stretching of -OH and -CH groups. The peaks observed at 550–650 and 1,000–1,500  $\text{cm}^{-1}$  are owing to the vibration of Fe-O and C=C vibration. As well as wide peaks around 1,620 and 2,500–3,300  $\text{cm}^{-1}$  region correspond to C=O and -COOH vibration [36]. As can be seen in Fig. 2(c), the nanocomposite shows saturation magnetization ( $M_s$ ) value of 6.7  $\text{emu g}^{-1}$ . Low  $M_s$  value can be attributed to the presence of the resin

onto the composite structure. The value of magnetic remnant ( $M_r$ ) for the nanocomposite was 0.01  $\text{emu g}^{-1}$ , which indicates that it possesses superparamagnetic properties because each particle is a single magnetic domain [37].

The  $\text{N}_2$  adsorption-desorption isotherm at Fig. 2(d) shows type II isotherm with a minor hysteresis loop as a result of filling and emptying of the mesopores by capillary condensation. According to the pore-size distribution curve, average pore size was 2.5 nm which indicates the magnetic polymer is mainly mesopores. Moreover, the specific surface area and pore volume for the nanocomposite were 173.96  $\text{m}^2 \text{g}^{-1}$  and 0.29  $\text{cm}^3 \text{g}^{-1}$ , respectively.

FE-SEM images (Figs. 3(a) and (b)) show fine regular uniform spheres with mean diameter of 90 nm. Sphere morphology is as a result of equivalent growth along the different directions of nucleation [38].

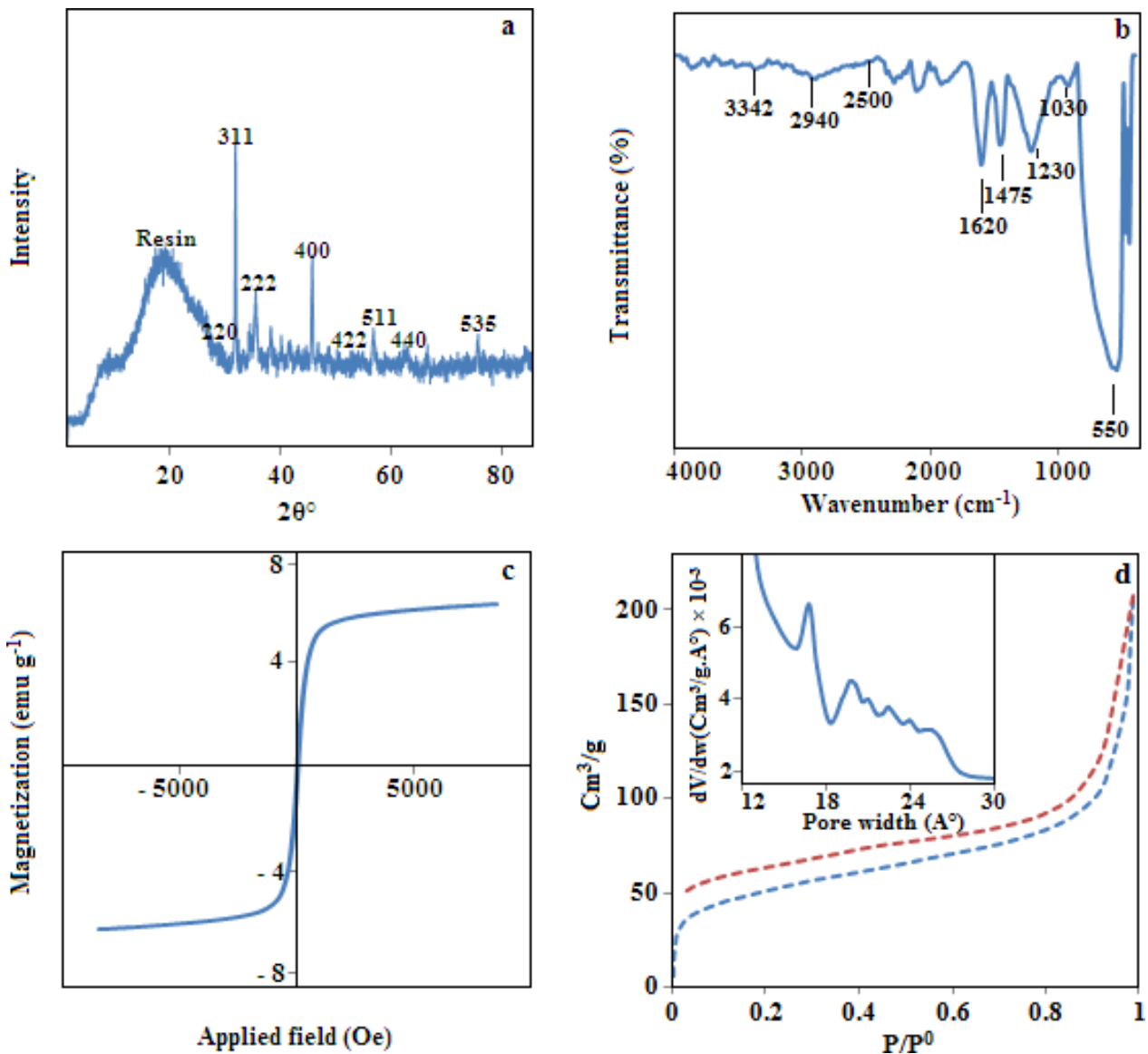


Fig. 2. The XRD pattern (a), FTIR (b), VSM graph, (c)  $\text{N}_2$  adsorption-desorption isotherm and pore width distribution (d) of as-synthesized magnetic resin.

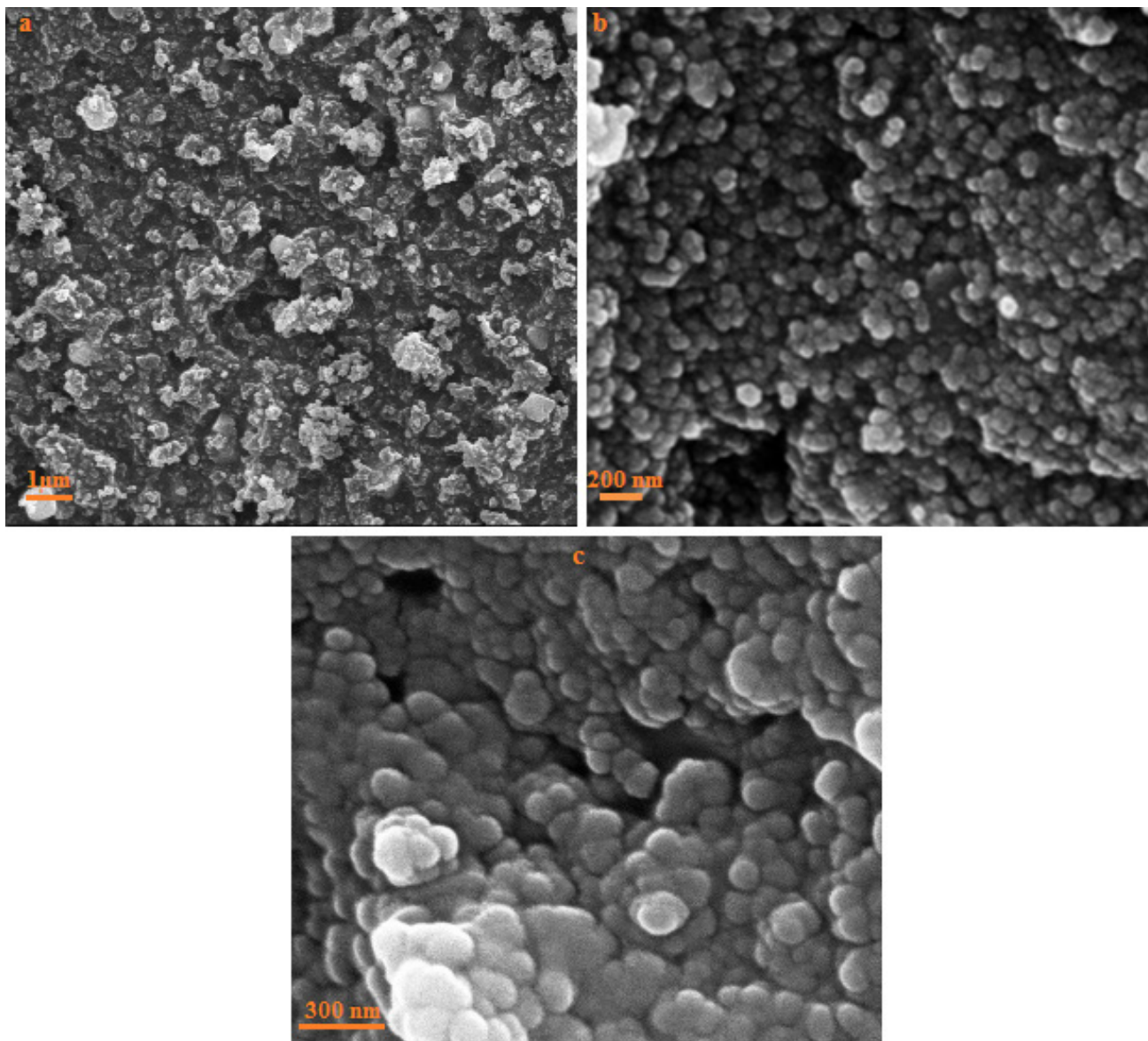


Fig. 3. The FE-SEM images of as-synthesized magnetic resin with various magnifications.

### 3.2. Removal experiments

#### 3.2.1. Effect of pH on dye adsorption

The influence of pH on CV adsorption was studied in the range of 2–10. For this purpose, 50 mL of CV solutions with a concentration of 10 mg L<sup>-1</sup> and adsorbent dosage of 50 mg were employed. After shaking for 10 min, the remained CV in the solution ( $C_e$ ; mg L<sup>-1</sup>) was determined and the removal percentage ( $R\%$ ) was calculated using the following equation:

$$R\% = (C_0 - C_e) \times 100 / C_0 \quad (2)$$

where  $C_0$  (mg L<sup>-1</sup>) is initial concentration of CV. Based on the results in Fig. 4(a), CV adsorption is in high level (95%) at acidic solution and reached to 99.55% at pH 10. This result indicates that CV adsorption onto resin surface is approximately independent from solution pH. Some increase in

adsorption removal at alkali solution is owing to the adsorption between the negatively charged sorbent (estimated based on  $pH_{pzc}$  in Fig. 4(b)) and cationic dye [39]. However, high adsorption efficiency in acidic solution confirms that various mechanisms participate simultaneously in CV adsorption. As known, CV is a triphenylmethane dye which contains benzene ring and C–C double bonds. The adsorbent also contain aromatic ring as a result hydrophobic interaction is a main mechanism for efficient uptake of CV by the nanohybrid. Other mechanisms include  $\pi$ – $\pi$  interactions between resin and aromatic backbones in CV structure. Hydrogen bonding between CV as a polar organic chemical and potential H-bonding sites (–OH) on the sorbent surface also participate in adsorption. Morphology of composite has also main role in capturing CV. Based on the BET data, as-synthesized composite possess pore areas between the fragments which is ready to capture CV molecules. In brief,  $\pi$ – $\pi$  interaction, hydrogen

bonding, electrostatic interaction as well as pore areas improve CV adsorption efficiency of the nano hybrid [40].

3.2.2. Effect of time

For studying the effect of time on CV adsorption 50 mL of sample solutions (10 mg L<sup>-1</sup>) containing 50 mg of the adsorbent have been shaken from 1.0 to 10 min and the CV concentration in supernatant has been determined. Results for effect of time on CV adsorption have been depicted in Fig. 4(c). As can be seen the sorbent showed fast adsorption kinetic as more than 96% of CV has been removed at first 1 min of reaction then complete removal obtained after 10 min. Fast equilibrium time is owing to the presence of high

amount of active sites on the nano hybrid structure which is easily accessible since exist in shallow zones of the sorbent. Finally equilibrium time of 10 min was selected to access high efficiency for CV adsorption.

3.2.3. Adsorbent dosage

Optimize the adsorbent dose could maximize the interactions between CV and adsorption sites of the magnetic resin. To investigate the effect of this parameter on the adsorption efficiency of CV, adsorbent amount has been varied from 5 to 40 mg and the process was performed on 50 mL of CV solutions with initial concentration of 10 mg L<sup>-1</sup>. According to the results (Fig. 5(a)), it is observed that the removal efficiency is

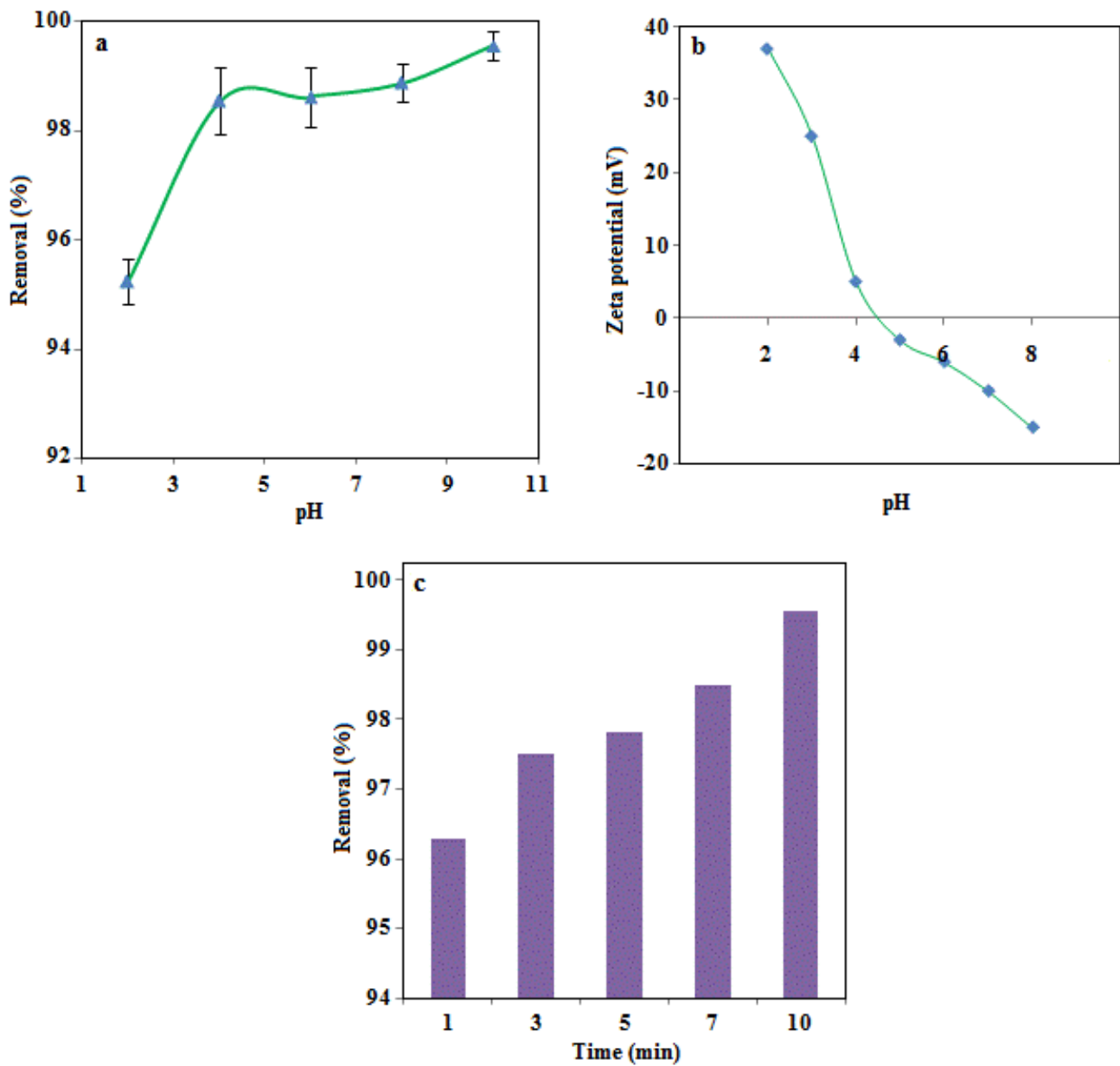


Fig. 4. Effect of pH on CV adsorption (a), the pattern of zeta potential for as-prepared magnetic resin (b) and effect of contact time (c) on CV adsorption by magnetic resin.

at high level (94.5%) with adsorbent amount of 5 mg. With increase in adsorbent dosage up to 30 mg the adsorption efficiency reached to 99% as a result this value was selected as optimum adsorbent dosage for CV adsorption. These results reveal that the adsorbent has good efficiency for dye removal since the adsorption efficiency is quantitative at low level of the sorbent which may be owing to the presence of various active sites (pore volume and benzenoid ring as well as hydroxyl functional groups) on the structure of nanohybrid.

### 3.2.4. Effect of ionic strength

The effect of ionic strength on CV adsorption with initial concentration of 10 mg L<sup>-1</sup> was studied at pH 8.0, adsorbent amount of 30 mg and time of 10 min. As shown in Fig. 5(b), adsorption of CV onto nanohybrid decreased upon addition of 1%–10% (w/v) of NaNO<sub>3</sub> salt. At the working pH, CV possess positive charge however the sorbent possess negative charge in other words, the sorbate–sorbent interaction accompanied with electrostatic attractive. It can be predicted that when the attractive electrostatic forces govern at the adsorption, an increase in ionic strength will decrease adsorption efficiency [41]. The experimental data from this study showed good agreement with the estimation as the decrease in dye removal observed after NaNO<sub>3</sub> addition.

### 3.3. Kinetic study

Effect of time on CV adsorption has been evaluated with kinetic models owing to the fact that changes in adsorption with time can be quantified by applying the appropriate model. Linearized form of the pseudo-first-order and pseudo-second-order models can be expressed by the following equations:

$$\ln(Q_c - Q_t) = \ln Q_c - K_1 t \quad (3)$$

$$t/Q_t = 1/(K_2 Q_c^2) + (1/Q_c)t \quad (4)$$

where  $K_1$  (min<sup>-1</sup>) and  $K_2$  (g mg<sup>-1</sup> min<sup>-1</sup>) are the pseudo-first-order and pseudo-second-order rate constant.  $Q_c$  and  $Q_t$  (mg g<sup>-1</sup>) correspond to the values of the amount adsorbed per unit mass at equilibrium and at any time  $t$ , respectively [42–44]. The values of constants can be determined experimentally from the slop and the intercept by plotting  $\ln(Q_c - Q_t)$  and  $t/Q_t$  vs.  $t$ . The plots of these kinetic models are shown in Figs. 6(a) and (b). Results (Table 1) indicate that the second-order plot has better linearity for CV adsorption, however, first-order model has linearity higher than 0.9. Further evaluation of the models based on the adsorption capacity indicated that the  $Q_c$  obtained based on the second-order model showed lower deviate from the experimental value relative to first-order model [45]. Moreover,  $\chi^2$  test [46] was used to determine best kinetic models.

$$\chi^2 = \sum \frac{(Q_{\text{exp}} - Q_c)^2}{Q_c} \quad (5)$$

Based on the results in Table 1, the second-order model showed lower  $\chi^2$  value relative to first-order model. Thus, the second-order model can be accepted as the kinetic mechanism for CV adsorption with the sorbent. In other words, chemisorption is the rate-controlling step since the second-order model is in agreement with chemisorption mechanism [47].

Kinetic models can be further evaluated with the intraparticle diffusion and liquid film model. Based on the intraparticle diffusion model (Eq. (5)), after transport of target analytes from the aqueous phase to the surface of the adsorbent, it diffuses into the interior of the porous particles [48,49]. Moreover, the liquid film diffusion model (Eq. (6)), explains the role of transport of the adsorbate from the liquid phase up to the solid phase boundary. These models can be written in the following equations:

$$Q_t = K_p t^{0.5} + C \quad (6)$$

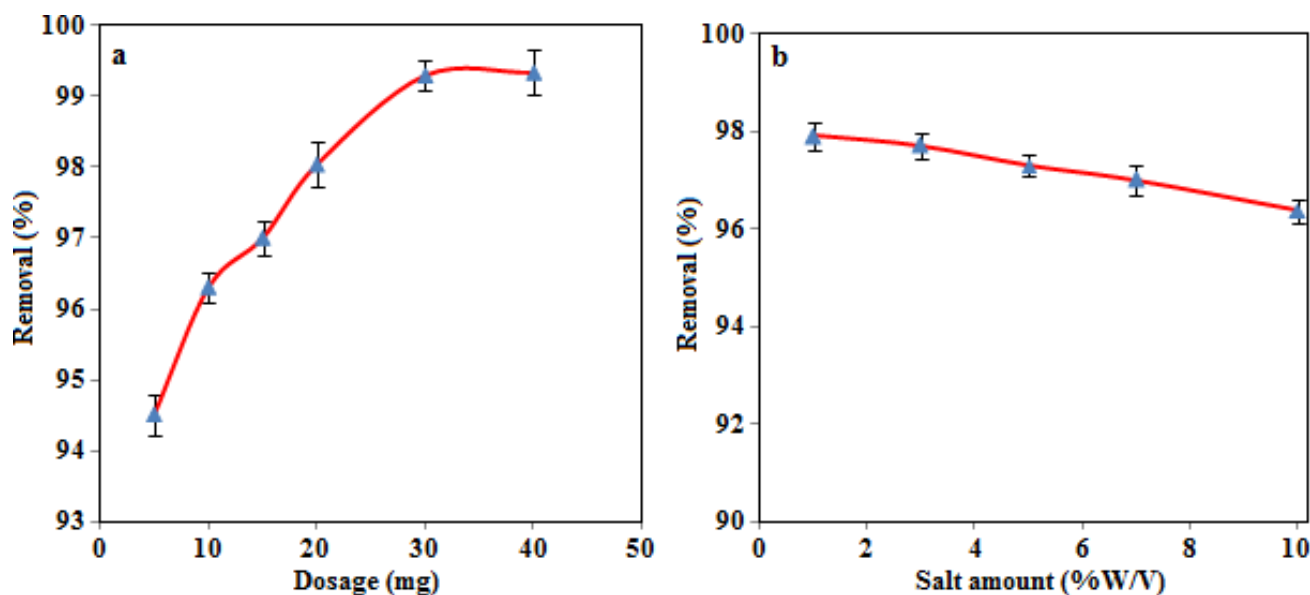


Fig. 5. Effect of adsorbent dosage (a) and ionic strength (b) on CV adsorption by magnetic resin.

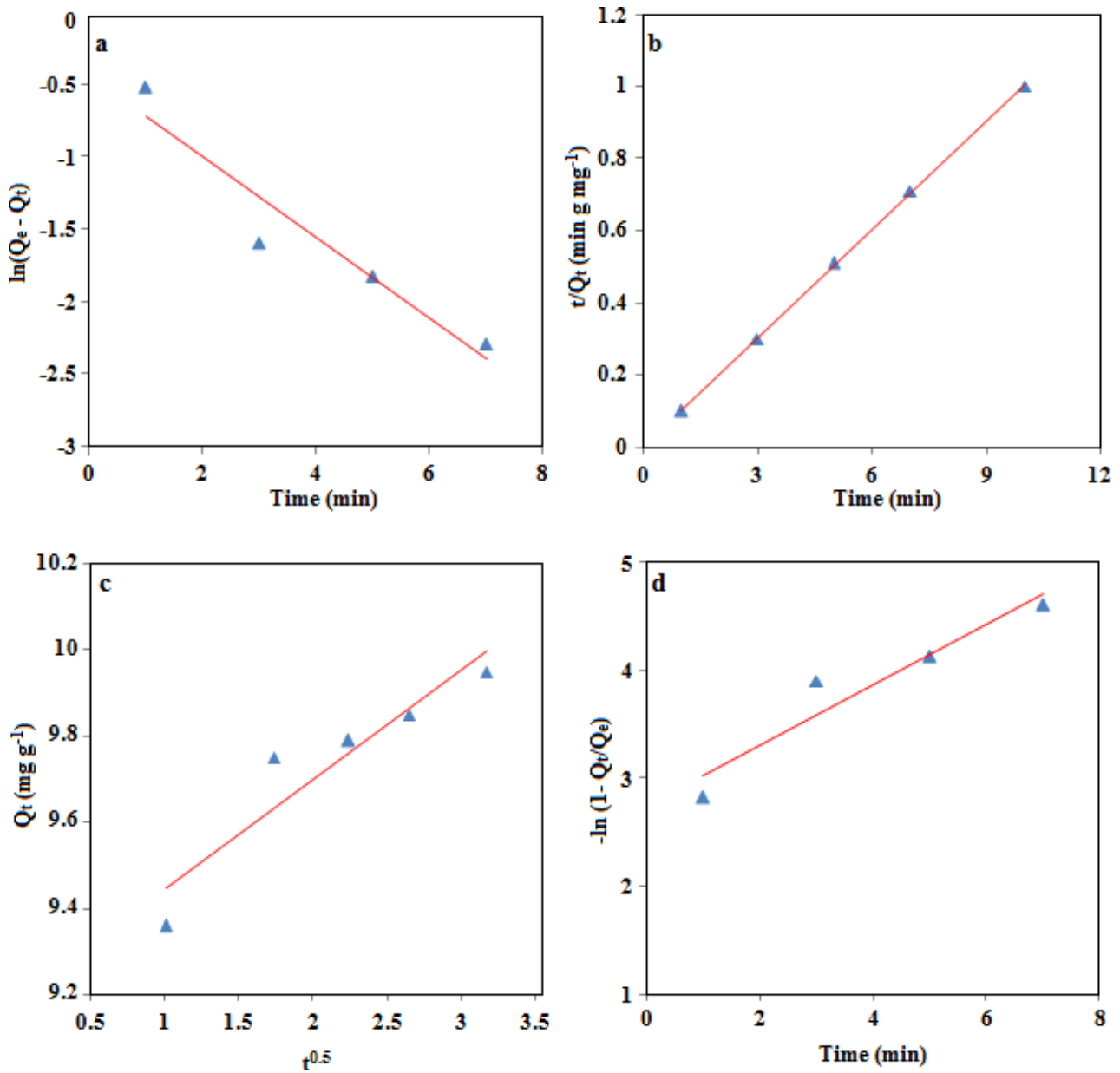


Fig. 6. The plot of first-order (a), second-order (b), intraparticle diffusion (c) and liquid film (d) model for CV adsorption by magnetic resin.

Table 1  
The data of kinetic models for adsorption of CV using magnetic resin

Model	Coefficient	Value	Model	Coefficient	Value
First-order	$R^2$	0.91	Diffusion model	$R^2$	0.88
	$K_1$	0.28		$K_p$	0.25
	$Q_e$	0.63		$C$	9.19
	$\chi^2$	2.31	Liquid film	$R^2$	0.91
Second-order	$R^2$	0.99		$K_{fd}$	0.27
	$K_2$	5		$C$	2.74
	$Q_e$	10			
	$Q_{exp}$	9.95			
	$\chi^2$	0.26			

$$\ln(1 - Q_t/Q_e) = -K_{fd}t \quad (7)$$

where  $K_p$  ( $\text{mg g}^{-1} \text{min}^{-0.5}$ ) represents diffusion rate constant,  $C$  gives information about the thickness of boundary layer and  $K_{fd}$  is the adsorption rate constant. According to the plot of  $Q_t$  against  $t^{0.5}$  (Fig. 6(c)), the model not shown good linearity ( $R^2 = 0.88$ ). Moreover, it has a high value of intercept which limits its application as rate-controlling step. The plot of  $-\ln(1 - Q_t/Q_e)$  vs.  $t$  (Fig. 6(d)) showed correlation coefficient value of 0.91 and the intercept value of 2.75 instead of zero predicted by the model. As a result, the role of film diffusion in the adsorption of CV can be dissembled.

Adsorption rate can be explained by the value of rate constants. As can be seen from the results in Table 1, the second-order model has high constant value ( $K_2 = 5$ ) which imply that CV adsorption takes place with high rate. Moreover, as can be seen liquid film model ( $K_{fd} = 0.27$ ) and intraparticle diffusion ( $K_p = 0.25$ ) possess low constant value. Low  $K_{fd}$  value exhibits that transport of the analyte from the liquid phase up to the boundary of the solid phase is slow. Moreover, low  $K_p$  value indicates that diffusion rate is slow which is owing to the fact that CV adsorption is along with pore diffusion instead of surface diffusion [50,51].

### 3.4. Adsorption isotherm

The results for effect of CV concentration on adsorption process are depicted in Fig. 7(a) and indicate that as-synthesized nanohybrid uptake more than 99% of the target analyte at an initial concentration of  $10 \text{ mg L}^{-1}$ . The removal efficiency decreased only a few percentage as it reached to 96.3% at an initial concentration of  $40 \text{ mg L}^{-1}$ . To estimate the efficiency of nanocomposite for dye removal, adsorption process was also performed in the presence of naked ferrite and polymer. Results at Fig. 7(a) showed that dye removal percentage is approximately same at an initial concentration of  $10 \text{ mg L}^{-1}$ . However, it can be seen that the removal percentage is around 75% using polymer and 60% of the ferrite nanoparticles at an initial concentration of  $40 \text{ mg L}^{-1}$  which reached to 96.3% using nanocomposite. This result confirms the efficiency of nanocomposite for dye removal.

To further understand the adsorption behavior of the nanocomposite, adsorption isotherms were also evaluated based on Langmuir and Freundlich model. The Langmuir model suggests that adsorption occurs at specific homogeneous monolayer surface and there is no interaction between adsorbate molecules. In other words, monolayer's adsorption confirms chemisorption which is responsible for the dye removing by the proposed sorbent [52,53], however, Freundlich model describes that multilayer adsorption occurs on a heterogeneous surface [54,55]. The linear Langmuir and Freundlich isotherm equation can be illustrated as follow:

$$C_e/Q_e = 1/(Q_m b) + C_e/Q_m \quad (8)$$

$$\ln Q_e = \ln K_f + 1/n \ln C_e \quad (9)$$

where  $C_e$ ,  $Q_e$ ,  $Q_m$ , and  $b$  are the equilibrium concentration ( $\text{mg L}^{-1}$ ), amount of adsorbed analyte at equilibrium ( $\text{mg g}^{-1}$ ), the maximum adsorption capacity of a monolayer ( $\text{mg g}^{-1}$ ), and the energy of adsorption ( $\text{L mg}^{-1}$ ), respectively. Moreover,

$K_f$  and  $n$  are Freundlich constants. A measure of adsorption favorability of Langmuir model,  $R_L$ , can be estimated with the followed equation:

$$R_L = 1/(1 + C_i b) \quad (10)$$

where  $C_i$  is the initial concentration of target analyte. The value of  $R_L$  indicated that Langmuir isotherm can be irreversible ( $R_L = 0$ ), favorable ( $0 < R_L < 1$ ), linear ( $R_L = 1$ ) or unfavorable ( $R_L > 1$ ). The results of Langmuir and Freundlich models are summarized in Table 2 and Figs. 7(b) and (c). It can be seen that experimental data fit with both models as values of  $R^2$  are more than 0.9, but, Freundlich model showed higher linearity relative to Langmuir model. The  $R_L$  value was found in the range of  $0 < R_L < 1$  (Table 2) which indicated Langmuir adsorption process is also favorable. The applicability of both isotherms shows that adsorption is along with monolayer process followed with multilayer adsorption on the surface of the adsorbent. In order to more accurate analysis of adsorption models,  $\chi^2$  test (Eq. (4)) was used to determine best isotherm models. According to the results (Table 2 and Fig. 7(d)), the Freundlich isotherm model shows a lower value of  $\chi^2$  test and higher nonlinear  $R^2$  value compared with the Langmuir isotherm and suggests that this model can better describe sorption behavior of dye.

### 3.5. Thermodynamic study

To study the effect of temperature on decolorization, the process has been performed at 50 mL volumetric flask with an initial dye concentration of  $10 \text{ mg L}^{-1}$  at 295, 303 and 318 K. According to the results at Fig. 8(a), dye adsorption increased with the increase of temperature which indicates that process is feasible at high temperature. The thermodynamic parameters for the adsorption process were evaluated and the values of  $\Delta H^\circ$  ( $\text{kJ mol}^{-1}$ ),  $\Delta S^\circ$  ( $\text{J K}^{-1} \text{mol}^{-1}$ ) and  $\Delta G^\circ$  ( $\text{kJ mol}^{-1}$ ) were calculated using the following equations:

$$\Delta G^\circ = -RT \ln(Q_e/C_e) \quad (11)$$

$$\Delta G^\circ = \Delta H^\circ - T\Delta S^\circ \quad (12)$$

$$\ln(Q_e/C_e) = \Delta S^\circ/R - \Delta H^\circ/RT \quad (13)$$

where  $R$  and  $T$  are gas constants ( $8.314 \times 10^{-3} \text{ kJ K}^{-1} \text{mol}^{-1}$ ) and absolute temperature (K), respectively. The plot of  $\ln(Q_e/C_e)$  vs.  $1/T$  is shown in Fig. 8(b) as the slope and the intercept giving values of  $\Delta H^\circ$  and  $\Delta S^\circ$  [56]. The results in Table 3 indicate that decolorization was accompanied by a decrease in the Gibbs energy ( $\Delta G^\circ$ ), which makes the interaction spontaneous. Entropy increased for dye adsorption as the value of  $\Delta S^\circ$  was positive. Moreover, positive enthalpy changes revealed endothermic adsorption path [57,58].

It is known that adsorption is a spontaneous process since it takes place by adsorbate getting adsorbed on adsorbent hence  $\Delta H^\circ$  has to be negative. In other words, owing to forces of attraction between adsorbate and adsorbent heat energy is released which confirm adsorption is an exothermic process. The result obtained in this work is in conflict with the mentioned rule ( $\Delta H^\circ = +3.52$ ). This is owing to the fact that

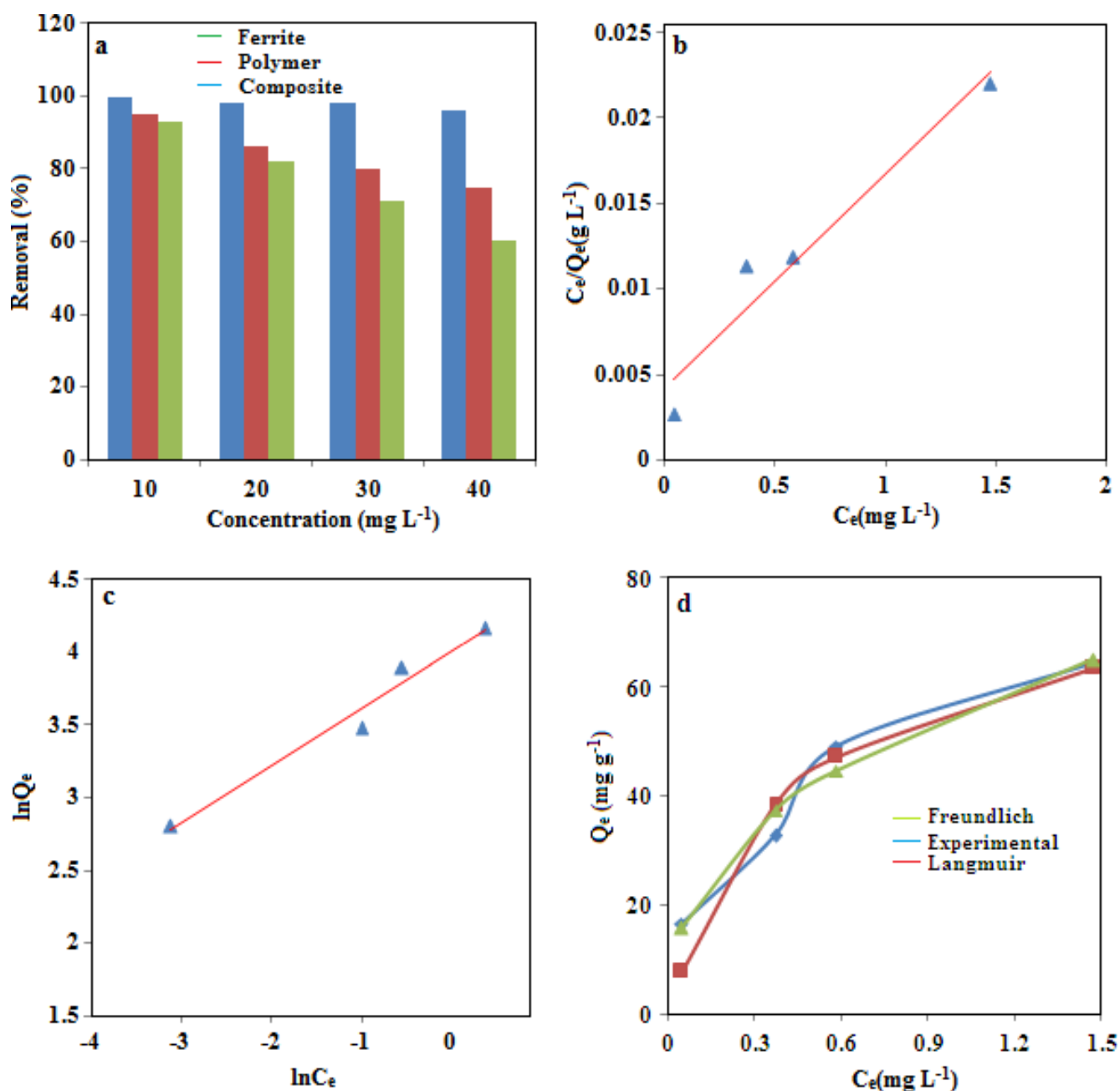


Fig. 7. Effect of initial CV concentration on CV adsorption efficiency of ferrite nanoparticles, polymer and nanocomposite (a), Langmuir isotherm (b), Freundlich isotherm model (c) and fitting experimental data with calculated values (d) for CV adsorption by magnetic resin.

adsorption from solution is governed by multiple adsorption steps including adsorbent–adsorbate, adsorbate–solvent and adsorbent–solvent interactions. In other words, the rise in temperature increases the pore diffusion through weakened the hydrogen bonds between solvent molecules and between solvent and adsorbate or adsorbent [59]. Therefore, increase in temperature assists dehydration of CV, which gives them a larger dipolar moment and enhances interactions with the sorbent. Moreover, at higher temperature the planarity of organic molecules increases which causes greater access to the microporosity of the sorbent [60]. As a result, CV

adsorption is endothermic because of endothermicity nature of dehydration process.

### 3.6. Regeneration

To make the adsorption process more economic, it is important that the sorbent could be regenerated. As a result, desorption experiments were studied using organic solvents such as methanol, ethanol, acetone and dimethyl sulfoxide. Selection of organic solvents was based on the fact that CV is an organic compound. In other words, its structure contains

benzene ring and other hydrophobic fragments which have a high affinity toward organic solvents. According to

Table 2  
The data of isotherm models for CV adsorption using magnetic resin

	$Q_m$ (mg g <sup>-1</sup> )	83.3
Langmuir	$R^2$	0.94
	$b$	3.0
	$R_L$	0.0087–0.034
	$\chi^2$	11.16
	$^aR^2$	0.91
	$n$	2.54
Freundlich	$K_f$	54.7
	$R^2$	0.97
	$\chi^2$	1.06
	$^aR^2$	0.96

<sup>a</sup>Nonlinear.

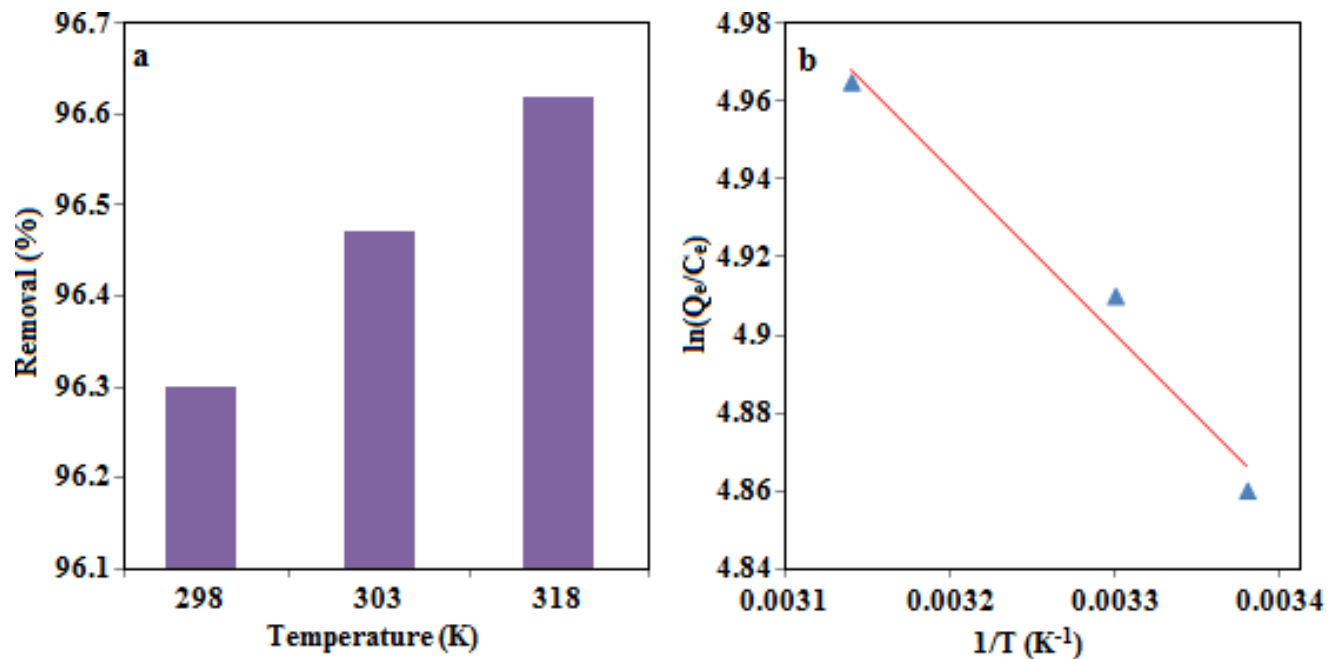


Fig. 8. Effect of temperature on CV adsorption (a) and plot of  $\ln K$  vs.  $1/T$  for CV adsorption by magnetic resin.

Table 4  
Comparison of CV adsorption by magnetic resin with some adsorbents reported in the literature

Sorbent	Time (min)	Adsorption capacity (mg g <sup>-1</sup> )	Reference
Plant waste	4 h	5.14	[1]
Calcium ferrite	30	10.67	[2]
Carboxylate cellulose	240	243.9	[6]
Nanoporous carbon	150	68.97	[10]
Formosa papaya seed	60	85.99	[14]
<i>Artocarpus odoratissimus</i> skin	150	195	[36]
ZnFe <sub>2</sub> O <sub>4</sub> resin	10	83.3	This work

the results, release efficiency was 64%, 62%, 52% and 55% using methanol, ethanol, acetone and dimethyl sulfoxide as eluent, respectively. It is known that CV is a cationic dye hence it assumes that acidic solution can assist dye release from the sorbent surface. Based on the  $pH_{pzc}$  study the sorbent possess positive charge at an acidic solution which can repulse cationic dye. Therefore, a mixture of nitric acid–methanol was also employed for dye release. It was found that elution efficiency was 90%. Hence, 5 mL of methanol–HNO<sub>3</sub> (0.1 mol L<sup>-1</sup>) mixture was used for dye release from sorbent surface.

Table 3  
The thermodynamic data for CV adsorption using magnetic resin

$\Delta G^\circ$ (kJ mol <sup>-1</sup> )			$\Delta H^\circ$ (kJ mol <sup>-1</sup> )	$\Delta S^\circ$ (J K <sup>-1</sup> mol <sup>-1</sup> )
295 K	303 K	318 K		
-11.91	-12.36	-13.11	+3.52	+52.37

### 3.7. Comparison with other methods

The present study for CV adsorption using magnetic polymeric resin has been compared with some reports in Table 4. It can be seen that the performances of the prepared nanocomposite are at the appropriate level since it demonstrates satisfactory sorption capacities as well as show low adsorption time. Moreover, the sorbent has been synthesized by one-step route hence it is a promising system for the removal of aqueous cationic dye to reduce its harmful effects on the environment.

### 4. Conclusions

The first report for one-step preparing zinc-ferrite@phenol-formaldehyde based polymeric resin and its application for CV adsorption has been demonstrated in this study. Prepared nanohybrid exhibited appropriate efficiency for cationic dye adsorption with good adsorption capacity ( $83.3 \text{ mg g}^{-1}$ ) and low equilibrium time of 10 min. Kinetic study showed that CV adsorption process followed the second-order model. The thermodynamic study proved that the adsorption is spontaneous with  $\Delta G^\circ = -11.91 \text{ kJ mol}^{-1}$  which followed endothermic pathway since  $\Delta H^\circ$  value is equal to  $+3.52 \text{ kJ mol}^{-1}$ . Moreover, adsorption process is accompanied by an increase in entropy ( $\Delta S^\circ = +52.37 \text{ J K}^{-1} \text{ mol}^{-1}$ ) which made the system entropy stabilized.

### Acknowledgment

Support of this investigation by the Research Council of Islamic Azad University, Arak branch through the grant is gratefully acknowledged.

### References

- [1] A. Mittal, J. Mittal, A. Malviya, D. Kaur, V.K. Gupta, Adsorption of hazardous dye crystal violet from wastewater by waste materials, *J. Colloid Interface Sci.*, 343 (2010) 463–473.
- [2] S. An, X. Liu, L. Yang, L. Zhang, Enhancement removal of crystal violet dye using magnetic calcium ferrite nanoparticle: study in single- and binary-solute systems, *Chem. Eng. Res. Des.*, 94 (2015) 726–735.
- [3] A. Nezamzadeh-Ejhi, H. Zabihi-Mobarakeh, Heterogeneous photodecolorization of mixture of methylene blue and bromophenol blue using CuO-nano-clinoptilolite, *J. Ind. Eng. Chem.*, 20 (2014) 1421–1431.
- [4] A. Nezamzadeh-Ejhi, M. Karimi-Shamsabadi, Decolorization of a binary azo dyes mixture using CuO incorporated nanozeolite-X as a heterogeneous catalyst and solar irradiation, *Chem. Eng. J.*, 228 (2013) 631–641.
- [5] Z. Chen, T. Wang, X. Jin, Z. Chen, M. Megharaj, R. Naidu, Multifunctional kaolinite-supported nanoscale zero-valent iron used for the adsorption and degradation of crystal violet in aqueous solution, *J. Colloid Interface Sci.*, 398 (2013) 59–66.
- [6] H. Qiao, Y. Zhou, F. Yu, E. Wang, Y. Min, Q. Huang, L. Pang, T. Ma, Effective removal of cationic dyes using carboxylate-functionalized cellulose nanocrystals, *Chemosphere*, 141 (2015) 297–303.
- [7] Y. Li, S. Yang, C. Sun, L. Wang, Q. Wang, Aqueous photofate of crystal violet under simulated and natural solar irradiation: kinetics, products, and pathways, *Water Res.*, 88 (2016) 173–183.
- [8] Q. Zhang, T. Zhang, T. He, L. Chen, Removal of crystal violet by clay/PNIPAm nanocomposite hydrogels with various clay contents, *Appl. Clay Sci.*, 90 (2014) 1–5.
- [9] R. Kumar, R. Ahmad, Biosorption of hazardous crystal violet dye from aqueous solution onto treated ginger waste (TGW), *Desalination*, 265 (2011) 112–118.
- [10] F. Güzel, H. Saygili, G.A. Saygili, F. Koyuncu, Decolorisation of aqueous crystal violet solution by a new nanoporous carbon: equilibrium and kinetic approach, *J. Ind. Eng. Chem.*, 20 (2014) 3375–3386.
- [11] M.B. Silveira, F.A. Pavan, N.F. Gelos, E.C. Lima, S.L.P. Dias, *Punica granatum* shell preparation, characterization, and use for crystal violet removal from aqueous solution, *Clean - Soil, Air, Water*, 42 (2014) 939–946.
- [12] Y. Pei, M. Wang, D. Tian, X. Xu, L. Yuan, Synthesis of core-shell SiO<sub>2</sub>@MgO with flower like morphology for removal of crystal violet in water, *J. Colloid Interface Sci.*, 453 (2015) 194–201.
- [13] S. Saber-Samandari, S. Saber-Samandari, S. Heydaripour, M. Abdouss, Novel carboxymethyl cellulose based nanocomposite membrane: synthesis, characterization and application in water treatment, *J. Environ. Manage.*, 166 (2016) 457–465.
- [14] F.A. Pavan, E.S. Camacho, E.C. Lima, G.L. Dotto, V.T.A. Branco, S.L.P. Dias, Formosa papaya seed powder (FPSP): preparation, characterization and application as an alternative adsorbent for the removal of crystal violet from aqueous phase, *J. Environ. Chem. Eng.*, 2 (2014) 230–238.
- [15] S. Chowdhury, S. Chakraborty, P.D. Saha, Response surface optimization of a dynamic dye adsorption process: a case study of crystal violet adsorption onto NaOH-modified rice husk, *Environ. Sci. Pollut. Res. Int.*, 20 (2013) 1698–1705.
- [16] B.C.S. Ferreira, F.S. Teodoro, A.B. Mageste, L.F. Gil, R.P. de Freitas, L.V.A. Gurgel, Application of a new carboxylate-functionalized sugarcane bagasse for adsorptive removal of crystal violet from aqueous solution: kinetic, equilibrium and thermodynamic studies, *Ind. Crops Prod.*, 65 (2015) 521–534.
- [17] W. Ma, X. Song, Y. Pan, Z. Cheng, G. Xin, B. Wang, X. Wang, Adsorption behavior of crystal violet onto opal and reuse feasibility of opal-dye sludge for binding heavy metals from aqueous solutions, *Chem. Eng. J.*, 193–194 (2012) 381–390.
- [18] W. Dai, H. Yu, N. Ma, X. Yan, Adsorption equilibrium and kinetic studies of crystal violet and naphthol green on torreyagrundis-skin-based activated carbon, *Korean J. Chem. Eng.*, 32 (2015) 335–341.
- [19] S.D. Khattri, M.K. Singh, Use of Sagaun sawdust as an adsorbent for the removal of crystal violet dye from simulated wastewater, *Environ. Prog. Sustain. Energy*, 31 (2012) 435–442.
- [20] A. Kaur, U. Gupta, A review on applications of nanoparticles for the preconcentration of environmental pollutants, *J. Mater. Chem.*, 19 (2009) 8279.
- [21] F. Chen, P. Fang, Y. Gao, Z. Liu, Y. Liu, Y. Dai, Effective removal of high-chroma crystal violet over TiO<sub>2</sub>-based nanosheet by adsorption-photocatalytic degradation, *Chem. Eng. J.*, 204–205 (2012) 107–113.
- [22] P. Monash, G. Pugazhenth, Adsorption of crystal violet dye from aqueous solution using mesoporous materials synthesized at room temperature, *Adsorption*, 15 (2009) 390–405.
- [23] J. Zolgharnein, M. Bagtash, T. Shariatmanesh, Simultaneous removal of binary mixture of Brilliant Green and Crystal Violet using derivative spectrophotometric determination, multivariate optimization and adsorption characterization of dyes on surfactant modified nano- $\gamma$ -alumina, *Spectrochim. Acta, Part A*, 137 (2015) 1016–1028.
- [24] C.J. Pandian, R. Palanivel, S. Dhananasekaran, Green synthesis of nickel nanoparticles using *Ocimum sanctum* and their application in dye and pollutant adsorption, *Chin. J. Chem. Eng.*, 23 (2015) 1307–1315.
- [25] B.A. Ünnü, G. Gündüz, M. Dükkancı, Heterogeneous Fenton-like oxidation of crystal violet using an iron loaded ZSM-5 zeolite, *Desal. Wat. Treat.*, 57 (2016) 11835–11849.
- [26] R.M. Mohamed, M.A. Barakt, Enhancement of photocatalytic activity of ZnO-SiO<sub>2</sub> by nano-sized Pt for efficient removal of dyes from wastewater effluents, *Int. J. Photoenergy*, 2012 (2012) 1–8.
- [27] A. Nezamzadeh-Ejhi, Z. Banan, Sunlight assisted photodecolorization of crystal violet catalyzed by CdS nanoparticles embedded on zeolite A, *Desalination*, 284 (2012) 157–166.

- [28] A. Nezamzadeh-Ejehieh, Z. Banan, A comparison between the efficiency of CdS nanoparticles/zeolite A and CdO/zeolite A as catalysts in photodecolorization of crystal violet, *Desalination*, 279 (2011) 146–151.
- [29] G. Zhang, C.S. Ni, L.J. Liu, G.X. Zhao, F. Fina, J.T.S. Irvine, Macro-mesoporous resorcinol-formaldehyde polymer resins as amorphous metal-free visible light photocatalysts, *J. Mater. Chem. A*, 3 (2015) 15413–15419.
- [30] S.R. Shirsath, A.P. Patil, B.A. Bhanvase, S.H. Sonawane, Ultrasonically prepared poly(acrylamide)-kaolin composite hydrogel for removal of crystal violet dye from wastewater, *J. Environ. Chem. Eng.*, 3 (2015) 1152–1162.
- [31] A. Pourjavadi, M. Nazari, S.H. Hosseini, Synthesis of magnetic graphene oxide-containing nanocomposite hydrogels for adsorption of crystal violet from aqueous solution, *RSC Adv.*, 5 (2015) 32263–32271.
- [32] K.P. Singh, S. Gupta, A.K. Singh, S. Sinha, Optimizing adsorption of crystal violet dye from water by magnetic nanocomposite using response surface modeling approach, *J. Hazard. Mater.*, 186 (2011) 1462–1473.
- [33] N.N. Nassar, N.N. Marei, G. Vitale, L.A. Arar, Adsorptive removal of dyes from synthetic and real textile wastewater using magnetic iron oxide nanoparticles: thermodynamic and mechanistic insights, *Can. J. Chem. Eng.*, 93 (2015) 1965–1974.
- [34] M. Davudabadi Farahani, F. Shemirani, Ferrofluid based dispersive-solid phase extraction for spectrophotometric determination of dyes, *J. Colloid Interface Sci.*, 407 (2013) 250–254.
- [35] C. Yao, Q. Zeng, G.F. Goya, T. Torres, J. Liu, H. Wu, M. Ge, Y. Zeng, Y. Wang, J.Z. Jiang, ZnFe<sub>2</sub>O<sub>4</sub> nanocrystals: synthesis and magnetic properties, *J. Phys. Chem. C*, 111 (2007) 12274–12278.
- [36] L.B.L. Lim, N. Priyantha, T. Zehra, C.W. Then, C.M. Chan, Adsorption of crystal violet dye from aqueous solution onto chemically treated *Artocarpus odoratissimus* skin: equilibrium, thermodynamics, and kinetics studies, *Desal. Wat. Treat.*, 57 (2015) 1–15.
- [37] A. Demir, R. Topkaya, A. Baykal, Green synthesis of superparamagnetic Fe<sub>3</sub>O<sub>4</sub> nanoparticles with maltose: its magnetic investigation, *Polyhedron*, 65 (2013) 282–287.
- [38] M.H. Beyki, H. Alijani, Y. Fazli, Green, fast and selective preconcentration of lead ions from various matrices using a novel magnetic sheet-like resin, *Anal. Methods*, 7 (2015) 9918–9927.
- [39] N. Arabpour, A. Nezamzadeh-Ejehieh, Modification of clinoptilolite nano-particles with iron oxide: increased composite catalytic activity for photodegradation of cotrimaxazole in aqueous suspension, *Mater. Sci. Semicond. Process.*, 31 (2015) 684–692.
- [40] B. Pan, B. Xing, Adsorption mechanisms of organic chemicals on carbon nanotubes, *Environ. Sci. Technol.*, 42 (2008) 9005–9013.
- [41] Y.S. Al-Degs, M.I. El-Barghouthi, A.H. El-Sheikh, G.M. Walker, Effect of solution pH, ionic strength, and temperature on adsorption behavior of reactive dyes on activated carbon, *Dyes Pigm.*, 77 (2008) 16–23.
- [42] P. Wang, Q. Ma, D. Hu, L. Wang, Removal of Reactive Blue 21 onto magnetic chitosan microparticles functionalized with polyamidoamine dendrimers, *React. Funct. Polym.*, 91–92 (2015) 43–50.
- [43] D. Sun, X. Zhang, Y. Wu, T. Liu, Kinetic mechanism of competitive adsorption of disperse dye and anionic dye on fly ash, *Int. J. Environ. Sci. Technol.*, 10 (2013) 799–808.
- [44] M. Borandegi, A. Nezamzadeh-Ejehieh, Enhanced removal efficiency of clinoptilolite nano-particles toward Co(II) from aqueous solution by modification with glutamic acid, *Colloids Surf., A*, 479 (2015) 35–45.
- [45] M. Heidari-Chaleshtori, A. Nezamzadeh-Ejehieh, Modified clinoptilolite nano-particles with aspartic acid for removal of Cu(II) from aqueous solutions: isotherms and kinetic aspects, *New J. Chem.*, 39 (2015) 9396–9406.
- [46] H. Alijani, Z. Shariatinia, A. Aroujalian Mashhadi, Water assisted synthesis of MWCNTs over natural magnetic rock: an effective magnetic adsorbent with enhanced mercury(II) adsorption property, *Chem. Eng. J.*, 281 (2015) 468–481.
- [47] M. Shirkhodaie, M. Hossein Beyki, F. Shemirani, Simple route synthesis of MnFe<sub>2</sub>O<sub>4</sub>@ alunitite composite for preconcentration of trace level of copper and lead from food and water samples, *Desal. Wat. Treat.*, 3994 (2016) 1–13.
- [48] M.H. Beyki, F. Shemirani, Dual application of facilely synthesized Fe<sub>3</sub>O<sub>4</sub> nanoparticles: fast reduction of nitro compound and preparation of magnetic polyphenylthiourea nanocomposite for efficient adsorption of lead ions, *RSC Adv.*, 5 (2015) 22224–22233.
- [49] D. Li, J. Yan, Z. Liu, Z. Liu, Adsorption kinetic studies for removal of methylene blue using activated carbon prepared from sugar beet pulp, *Int. J. Environ. Sci. Technol.*, 13 (2016) 1815–1822.
- [50] T. Tarawou, E. Young, Intraparticle and liquid film diffusion studies on the adsorption of Cu<sup>2+</sup> and Pb<sup>2+</sup> ions from aqueous solution using powdered cocoa pod (*Theobroma cacao*), *Int. Res. J. Eng. Technol.*, 2 (2015) 236–243.
- [51] I. Uzun, Kinetics of the adsorption of reactive dyes by chitosan, *Dyes Pigm.*, 70 (2006) 76–83.
- [52] M. Anari-Anaraki, A. Nezamzadeh-Ejehieh, Modification of an Iranian clinoptilolite nano-particles by hexadecyltrimethyl ammonium cationic surfactant and dithizone for removal of Pb(II) from aqueous solution, *J. Colloid Interface Sci.*, 440 (2015) 272–281.
- [53] H. Shirzadi, A. Nezamzadeh-Ejehieh, An efficient modified zeolite for simultaneous removal of Pb(II) and Hg(II) from aqueous solution, *J. Mol. Liq.*, 230 (2017) 221–229.
- [54] S.M. Sayyah, A.A. Essawy, A.M. El-Nggar, Kinetic studies and grafting mechanism for methyl aniline derivatives onto chitosan: highly adsorptive copolymers for dye removal from aqueous solutions, *React. Funct. Polym.*, 96 (2015) 50–60.
- [55] A. Nematollahzadeh, A. Shojaei, M. Karimi, Chemically modified organic/inorganic nanoporous composite particles for the adsorption of reactive black 5 from aqueous solution, *React. Funct. Polym.*, 86 (2015) 269–281.
- [56] X. Ren, W. Xiao, R. Zhang, Y. Shang, R. Han, Adsorption of crystal violet from aqueous solution by chemically modified phoenix tree leaves in batch mode, *Desal. Wat. Treat.*, 53 (2015) 1324–1334.
- [57] A. Naghash, A. Nezamzadeh-Ejehieh, Comparison of the efficiency of modified clinoptilolite with HDTMA and HDP surfactants for the removal of phosphate in aqueous solutions, *J. Ind. Eng. Chem.*, 31 (2015) 185–191.
- [58] A. Nezamzadeh-Ejehieh, M. Kabiri-Samani, Effective removal of Ni(II) from aqueous solutions by modification of nano particles of clinoptilolite with dimethylglyoxime, *J. Hazard. Mater.*, 260 (2013) 339–349.
- [59] A.P. Terzyk, Molecular properties and intermolecular forces – factors balancing the effect of carbon surface chemistry in adsorption of organics from dilute aqueous solutions, *J. Colloid Interface Sci.*, 275 (2004) 9–29.
- [60] M.A. Fontecha-Camara, M.V. Lopez-Ramon, M.A. Alvarez-Merino, C. Moreno-Castilla, About the endothermic nature of the adsorption of the herbicide diuron from aqueous solutions on activated carbon fiber, *Carbon*, 44 (2006) 2335–2338.